Materials Physics and Mechanics 44 (2020) 392-403 Received: January 28, 2020

FINITE ELEMENT HOMOGENIZATION OF PIEZOCOMPOSITES WITH ISOLATED INCLUSIONS USING IMPROVED 3-0 ALGORITHM FOR GENERATING REPRESENTATIVE VOLUMES IN ACELAN-COMPOS PACKAGE

A.B. Kudimova[1], D.K. Nadolin[1], A.V. Nasedkin[1*], A.A. Nasedkina[1], P.A. Oganesyan[1], A.N. Soloviev[1,2]

[1]Institute of Mathematics, Mechanics and Computer Science, Southern Federal University, Miltchakova str., 8a, Rostov on Don 344090, Russia

[2]Department of Theoretical and Applied Mechanics, Don State Technical University, 344000 Rostov-on-Don, Russia

*e-mail: nasedkin@math.sfedu.ru

Abstract. The paper considers the homogenization problems on the determination of the effective moduli of piezoceramic materials with elastic inclusions. The numerical solutions have been obtained by the effective moduli method and finite element method for the representative volumes with granular inclusions created in ACELAN-COMPOS package according to the original 3-0 algorithm. New features of this algorithm allow the user to vary different characteristics of the generated granules. The provided examples of finite element computations illustrate the influence of the shapes of granules and their locations on the effective properties of piezocomposites.

Keywords: piezoelectricity, two-phase piezocomposite, inclusion, effective modulus, representative volume, finite element method, finite element software, ACELAN-COMPOS

1. Introduction

Composite piezoceramic materials have found wide practical applications in the recent years [1,2]. At the stage of production of these piezoceramic materials, the properties of the input substances and technological features of the production process can be varied in order to obtain composite materials with optimal properties for specific applications. [3]. The mathematical modeling methods enable us to carry out computer design of the piezocomposite, thus helping to reduce the number of full-scale experiments necessary for creating the composite with required characteristics.

As it was noted in many papers (see [4-11], for instance) the piezocomposite properties considerably depend not only on material parameters and percentage of the input material phases but also on the distribution of these phases in the composite volume. The finite element package ACELAN-COMPOS [12-14] was specially developed for the analysis of the properties of dielectric, elastic, piezoelectric, and magnetoelectric composites of different connectivity types.

The determination of the piezocomposite effective properties in ACELAN-COMPOS package was done by solving the homogenization problems for the representative volume

http://dx.doi.org/10.18720/MPM.4432020_10

using the effective moduli method and the finite element method. In order to take into account the internal structure of the composite, a range of original algorithms was developed and introduced in ACELAN-COMPOS for generating representative volumes with special properties of the composite phases. The paper describes new features of the algorithm for generating the representative volumes with granular inclusions or pores. The representative volume obtained by this algorithm has a 3-0 connectivity by R. Newnham [15] terminology when the material of the main phase can spread between the edges of the composite in three perpendicular directions, and the second phase comprises isolated inclusions or pores. New features of the algorithm enable the user to generate the composite structures with controlled characteristics of granular inclusions. To continue investigations presented in [16-18], here we present the computation results for ceramic matrix piezocomposites for different types of granular inclusions.

2. Mathematical models and the effective moduli method

Mathematical statements of the homogenization problems for mixture piezoelectric composites by the effective moduli method have been described in a range of papers [16-18]. In this section, we will formulate this problem statement in slightly different from [16-18] but equivalent form. These statements of the homogenization problems are used in ACELAN-COMPOS package for the effective moduli computation of two-component (two-phase) piezoelectric composite materials. Let Ω be a representative volume of such composite, $\Gamma = \partial\Omega$ is the boundary of this volume, $\mathbf{n}$ is the outer unit normal vector to Γ, $\mathbf{u} = \mathbf{u}(\mathbf{x})$ is the vector-function of displacements, $\varphi = \varphi(\mathbf{x})$ is the function of electric potential, $\mathbf{x} = \{x_1, x_2, x_3\}$ is the vector of space coordinates. Let us consider that the volume Ω is subdivided into two subsets $\Omega = \Omega^{(1)} \cup \Omega^{(2)}$, occupied by two piezoelectric materials with different physico-mechanical properties, where the volume $\Omega^{(1)}$ is filled with the main piezoelectric material, i. e. is the composite skeleton (matrix), and the volume $\Omega^{(2)}$ is the set of inclusions or pores and is filled with other material. We will consider the second material as piezoelectric even in the cases when it is elastic or porous. For such materials, we will set negligibly small piezomoduli, and for the pores, we can also set negligibly small stiffnesses.

In order to define the full set of the effective moduli for the piezoelectric composite in ACELAN-COMPOS package, we solve the following nine ($k = 1, 2, ..., 9$) boundary-value problems:

$$\mathbf{\Lambda}^{\mathrm{T}}(\nabla) \cdot \mathbf{\Xi} = 0, \quad \mathbf{\Xi} = \mathbf{\Pi} \cdot \mathbf{Z}, \quad \mathbf{Z} = \mathbf{\Lambda}(\nabla) \cdot \mathbf{A}, \quad \mathbf{x} \in \Omega, \tag{1}$$

$$\mathbf{\Lambda}^{\mathrm{T}}(\nabla) = \begin{bmatrix} \partial_1 & 0 & 0 & 0 & \partial_3 & \partial_2 & 0 & 0 & 0 \\ 0 & \partial_2 & 0 & \partial_3 & 0 & \partial_1 & 0 & 0 & 0 \\ 0 & 0 & \partial_3 & \partial_2 & \partial_1 & 0 & 0 & 0 & 0 \\ 0 & 0 & 0 & 0 & 0 & 0 & -\partial_1 & -\partial_2 & -\partial_3 \end{bmatrix}, \quad \nabla = \begin{Bmatrix} \partial_1 \\ \partial_2 \\ \partial_3 \end{Bmatrix}, \quad \mathbf{A} = \begin{Bmatrix} u_1 \\ u_2 \\ u_3 \\ \varphi \end{Bmatrix}, \tag{2}$$

$$\mathbf{\Pi} = \begin{bmatrix} c_{11}^E & c_{12}^E & c_{13}^E & c_{14}^E & c_{15}^E & c_{16}^E & -e_{11} & -e_{31} & -e_{31} \\ c_{21}^E & c_{22}^E & c_{23}^E & c_{24}^E & c_{25}^E & c_{36}^E & -e_{12} & -e_{22} & -e_{32} \\ c_{31}^E & c_{32}^E & c_{33}^E & c_{34}^E & c_{35}^E & c_{36}^E & -e_{13} & -e_{23} & -e_{33} \\ c_{41}^E & c_{42}^E & c_{43}^E & c_{44}^E & c_{45}^E & c_{46}^E & -e_{14} & -e_{24} & -e_{34} \\ c_{51}^E & c_{52}^E & c_{53}^E & c_{54}^E & c_{55}^E & c_{56}^E & -e_{15} & -e_{25} & -e_{35} \\ c_{61}^E & c_{62}^E & c_{63}^E & c_{64}^E & c_{65}^E & c_{66}^E & -e_{16} & -e_{26} & -e_{36} \\ e_{11} & e_{12} & e_{13} & e_{14} & e_{15} & e_{16} & \varepsilon_{11}^S & \varepsilon_{12}^S & \varepsilon_{13}^S \\ e_{21} & e_{22} & e_{23} & e_{24} & e_{25} & e_{26} & \varepsilon_{21}^S & \varepsilon_{22}^S & \varepsilon_{23}^S \\ e_{31} & e_{32} & e_{33} & e_{34} & e_{35} & e_{36} & \varepsilon_{31}^S & \varepsilon_{32}^S & \varepsilon_{33}^S \end{bmatrix}, \quad \mathbf{\Xi} = \begin{Bmatrix} \sigma_{11} \\ \sigma_{22} \\ \sigma_{33} \\ \sigma_{23} \\ \sigma_{13} \\ \sigma_{12} \\ D_1 \\ D_2 \\ D_3 \end{Bmatrix}, \quad \mathbf{Z} = \begin{Bmatrix} \varepsilon_{11} \\ \varepsilon_{22} \\ \varepsilon_{33} \\ 2\varepsilon_{23} \\ 2\varepsilon_{13} \\ 2\varepsilon_{12} \\ E_1 \\ E_2 \\ E_3 \end{Bmatrix}, \tag{3}$$

$$\mathbf{A} = \mathbf{\Lambda}^{\mathrm{T}}(\mathbf{x}) \cdot \mathbf{Z}_{0\zeta}, \qquad \zeta = 1, 2, ..., 9, \qquad \mathbf{x} \in \Gamma, \tag{4}$$

where $\mathbf{Z}_{0\zeta}$ is the nine-dimensional array, in which all components are equal to zero, except the component with the number ζ, which equals some constant value S_0 for $\zeta = 1, 2, ..., 6$, and equals some constant value E_0 for $\zeta = 7, 8, 9$ (in a dimensionless problem setting the values S_0 and E_0 can be taken equal to one).

Here in (1)–(4) σ_{ij} are the components of the stress tensor; ε_{ij} are the components of the strain tensor; D_i are the components of the electric induction vector; E_i are the components of the electric field density vector; $c_{\alpha\beta}^E$ are the effective stiffness moduli measured at constant (zero) electric field; $e_{i\beta}$ are the piezomoduli (piezoelectric stress constants); ε_{ij}^S are the dielectric permittivity coefficients measured at constant (zero) strains; $\alpha, \beta = 1, 2, ..., 6$; $i, j = 1, 2, 3$; $(...)^{\mathrm{T}}$ is the transposition operation; and $(...) \cdot (...)$ denotes the inner product.

We note that in problems (1)–(4) the material moduli in the volume Ω are piece-wise continuous: $c_{\alpha\beta}^E = c_{\alpha\beta}^{E(l)}$, $e_{i\beta} = e_{i\beta}^{(l)}$, $\varepsilon_{ij}^S = \varepsilon_{ij}^{S(l)}$ for $\mathbf{x} \in \Omega^{(l)}$, $l = 1, 2$.

After obtaining solutions $(u_1)_\zeta$, $(u_2)_\zeta$, $(u_3)_\zeta$, $(\varphi)_\zeta$, for each of the problems (1)–(4) with $\zeta = 1, 2, ..., 9$ we calculate the components of the stress tensor $(T_1)_\zeta = (\sigma_{11})_\zeta$, $(T_2)_\zeta = (\sigma_{22})_\zeta$, $(T_3)_\zeta = (\sigma_{33})_\zeta$, $(T_4)_\zeta = (\sigma_{23})_\zeta$, $(T_5)_\zeta = (\sigma_{13})_\zeta$, $(T_6)_\zeta = (\sigma_{12})_\zeta$, and the components of the electric induction vector $(D_i)_\zeta$ in the volume Ω. Further, we find the average values for these quantities by the formula

$$< (...) >= \frac{1}{|\Omega|} \int_\Omega (...) d\Omega. \tag{5}$$

The averaged values enable us to obtain the full set of effective moduli $c_{\alpha\beta}^{E\,\mathrm{eff}}$, $e_{i\beta}^{\mathrm{eff}}$, $\varepsilon_{ij}^{S\,\mathrm{eff}}$ for the piezoelectric composite material. Indeed, from the solutions of problems (1)–(4) for $\zeta = 1, 2, ..., 6$ we determine the effective stiffness moduli $c_{\alpha\zeta}^{E\,\mathrm{eff}}$ and the effective piezomoduli $e_{i\zeta}^{\mathrm{eff}}$

$$c_{\alpha\zeta}^{E\,\mathrm{eff}} = \left\langle (T_\alpha)_\zeta \right\rangle / S_0, \quad \alpha = 1, 2, ..., 6; \qquad e_{i\zeta}^{\mathrm{eff}} = \left\langle (D_i)_\zeta \right\rangle / S_0, \quad i = 1, 2, 3. \tag{6}$$

The solutions of problems (1)–(4) for $\zeta = 7, 8, 9$ help to verify the effective piezomoduli $e_{k\alpha}^{\text{eff}}$ and determine the effective moduli of dielectric permittivities $\varepsilon_{ik}^{S\,\text{eff}}$ when $k = \zeta - 6$, i.e. $k = 1, 2, 3$:

$$e_{k\alpha}^{\text{eff}} = -\left\langle (T_\alpha)_\zeta \right\rangle / E_0, \quad \alpha = 1, 2, ..., 6; \qquad \varepsilon_{ik}^{S\,\text{eff}} = \left\langle (D_i)_\zeta \right\rangle / E_0, \quad i = 1, 2, 3. \tag{7}$$

The detailed formulation of the effective moduli method for piezoelectric composites described here was given in [19], as well as in [14] for the more general case of thermomagnetoelectric composites. For ordinary piezoceramic composite materials the corresponding piezomoduli calculated by (6) and (7) coincide up to numerical errors, and the matrices of the effective stiffness moduli and dielectric permittivities are symmetric: $c_{\alpha\beta}^{E\,\text{eff}} \approx c_{\beta\alpha}^{E\,\text{eff}}$, $\varepsilon_{ij}^{S\,\text{eff}} \approx \varepsilon_{ji}^{S\,\text{eff}}$. Besides, in the absence of geometric anisotropy in the phases distribution in the representative volume, the effective moduli preserve the structures of the general classes of anisotropy of the individual phases moduli.

3. Peculiarities of solving homogenization problems in ACELAN-COMPOS

Boundary value problems (1)-(4) in the ACELAN-COMPOS package are solved by the finite element method. The finite element systems of linear algebraic equations solved in ACELAN-COMPOS have the block form standard for piezoelectric problems [14,19]

$$\mathbf{K} \cdot \mathbf{X} = \mathbf{F}, \qquad \mathbf{K} = \begin{bmatrix} \mathbf{K}_{uu} & \mathbf{K}_{u\varphi} \\ \mathbf{K}_{u\varphi}^{\mathrm{T}} & -\mathbf{K}_{\varphi\varphi} \end{bmatrix}, \qquad \mathbf{F} = \begin{Bmatrix} \mathbf{F}_u \\ -\mathbf{F}_\varphi \end{Bmatrix}, \qquad \mathbf{X} = \begin{Bmatrix} \mathbf{U} \\ \mathbf{\Phi} \end{Bmatrix}, \tag{8}$$

where $\mathbf{U}$ is the vector of nodal displacements; $\mathbf{\Phi}$ is a vector of nodal electric potentials; $\mathbf{K}_{uu}$ is a finite element stiffness matrix; $\mathbf{K}_{u\varphi}$ is a finite element matrix of piezoelectric moduli; $\mathbf{K}_{\varphi\varphi}$ is a finite element permittivity matrix. The vectors of the right-hand sides $\mathbf{F}_u$ and $\mathbf{F}_\varphi$ appear in (8) after the essential boundary conditions (4) are taken into account. Here, the matrices $\mathbf{K}_{uu}$ and $\mathbf{K}_{\varphi\varphi}$ are both symmetric and positive definite and as a result, the matrix of the system $\mathbf{K}$ in (8) is quasi-definite or a saddle structure matrix [20,21].

The matrix $\mathbf{K}$ is stored in a sparse form. A column-oriented format is used, in which nonzero values in the columns are sorted in increasing row order. To solve the system of equations (8) в ACELAN-COMPOS a solver can be selected from iterative LSQR algorithm [22,23], and direct solver from external CSPARSE library, which implements LU decomposition [24].

Representative volumes of two-phase mixed composites are created in ACELAN-COMPOS in the form of regular finite element grids consisting of cubic finite elements Ω_{em} of the equal types and sizes oriented parallel to the coordinate axes (*m* is an element number).

Therefore, for a two-phase composite, the elemental matrices $\mathbf{K}_{em}$ are the same for all elements of the first phase, so $\mathbf{K}_{em} = \mathbf{K}_{em}^{(1)} = \mathbf{K}_e^{(1)}$ for the elements $\Omega_{em}^{(1)}$ of the first phase, and are the same for all elements of the second phase, so $\mathbf{K}_{em} = \mathbf{K}_{em}^{(2)} = \mathbf{K}_e^{(2)}$ for the elements $\Omega_{em}^{(2)}$ of the second phase. The global matrix of system (8) is constructed in ACELAN-COMPOS as a result of the standard procedure of elemental matrices assembly

$$\mathbf{K} = \sum_m^a \mathbf{K}_{em}^{(l)}, \tag{9}$$

where $\sum_m^a$ denotes an assembly operation, i.e. an assembly of the global finite element matrix from element matrices. Then, obviously, in the assembly process (9), only two precomputed matrices $\mathbf{K}_e^{(l)}$, $l = 1, 2$ can be used, which provides a significant acceleration of

the assembly procedure. To calculate the matrices $\mathbf{K}_e^{(l)}$ in ACELAN-COMPOS, you can choose one of the two available types of piezoelectric elements: a trilinear hexahedron with 8 nodes HEX8 and serendipity three-quadratic hexahedron HEX20 with 20 nodes. For canonical grids with cubic elements parallel to the coordinate axes, there is no need to use the isoparametric form of these elements, and all calculations can be performed in the original Cartesian coordinate system. Both in the calculation of elemental matrices $\mathbf{K}_e^{(l)}$ and in the post-processor calculations of effective moduli according to (5)–(7), ACELAN-COMPOS uses standard cubature formulas for numerical integration over cubic finite elements with 8 and 14 nodes [25].

4. Improved 3-0 algorithm ACELAN-COMPOS

The finite element mesh of the representative volume in ACELAN-COMPOS package is divided into domains, which are located uniformly along the coordinate axes. The domain is considered to be a minimal representative volume, which can contain the given connectivity structure. The domain has the shape of a cube and consists of cubic finite elements. The size of the domain is the number of elements along one of the coordinate axes, which can be defined by the user. The minimal domain has a size equal to 8 and consists of $8^3 = 512$ elements. Larger domains have the sizes that are multiples of 8, for example, 16, 32, and so on.

The previous algorithm of the 3-0 connectivity representative volume generation implemented in ACELAN-COMPOS was described in detail in [13,18]. This algorithm works independently inside every domain. In the beginning, all elements of the domain have piezoelectric material properties of the main material of the first phase. During the run of the algorithm, the material properties of the corresponding finite elements are changed to the material properties of the material of the second phase. The algorithm creates isolated inclusions inside the domain. The input parameters for the algorithm are the target percentage of inclusions and the minimal and maximal sizes of the granules. Here and after the granule size denotes the number of the elements constituting the granule. The minimal size of the granule is checked upon adding every new granule: if the granule of minimal size cannot be added to the current representative volume without violating other requirements, the process stops.

Schematically, the work of the algorithm can be described by the following steps:

1. Randomly select the finite element of the domain with the material properties of the material of the first phase and place the granule of size 1 inside it;
2. Let the granule grow while either its size does not exceed the maximal granule size, or the granule can be expanded without violating the connectivity of the material, or the target percentage of inclusions has not been reached.
3. If the target percentage of inclusions is not reached, return to step 1.

As a result of the execution of the algorithm, the requirements for minimal and maximal sizes of the granules can be sometimes not satisfied with the desired precision. Separate granules can merge, forming one large granule, the size of which can be larger than the input maximal size. The cases, when the granules are formed at the edges of the domain, can also lead to the generation of the granules in the representative volume, which size is larger than the given maximal size. When the granules spread to the edges of the domain, the resulting structure of the representative volume can violate the requirements for 3-0 connectivity, which represents the main disadvantage of the algorithm.

A new improved 3-0 algorithm attempts to correct the flaws of the previous version by introducing a number of constraints. Three types of constraints were implemented in the new version of the algorithm. The first constraint prohibits the granule elements to be located at

the domain edges, which guarantees 3-0 connectivity for the whole set of domains. The second constraint prohibits the granules to merge, which does not allow the algorithm to generate glued granules that exceed the maximal given size. The third constraint combines the first and second types, which enable generating the 3-0 connectivity structure with the granules that do not exceed the maximal size.

However, we note that in the case of the ban on generating the granules at the domain edges, the representative volume will contain a regular mesh of the elements of the main material on the boundaries between the domains, which gives additional stiffness to the whole structure and does not exactly represent a random arrangement of the granules.

Additional conditions on the possible arrangement of the granules limit the maximal percentage of inclusions that can be generated in the representative volume. For example, if the granule size is set to be from 5 to 10 elements, the algorithm without constraints creates representative volumes with up to 89 % of inclusions. The ban on merging the granules inside the domain limits the maximal percentage of inclusions to 21 %. With the ban on merging the granules between the domains, the maximal percentage of inclusions will be limited to 38 %, whereas the total ban on merging the granules will limit the maximal percentage of inclusions to 10 %. These estimations were obtained for minimal domain size. Increasing the number of elements in the domain enables the algorithm to increase the maximal achievable percentage of inclusions and generate the meshes that exactly match the corresponding input data. For example, if we increase the number of elements in each domain to $16^3 = 4096$, then for the same conditions and the same maximal granule size the maximal percentage of inclusions will increase to 13.75 %. The choice of the constraint type should be related to the real composite structure and depend on the geometric characteristics of the inclusions and on the methods of the composite production.

Figures 1 and 2 represent examples of the representative volumes obtained for four versions of the algorithm: (*a*) without constraints; (*b*) with the ban on the granules merging inside the domain; (*c*) with the ban on the granules merging between the domains; (*d*) with the ban on any type of the granules merging. In Figure 1, the representative volumes consist of eight domains with the size equal to 8, and in Fig. 2 the representative volumes consist of one domain with the size equal to 16. Thus, the representative volumes shown in Figs. 1 and 2 contain the same number of finite elements equal to $16^3 = 4096$. In order to demonstrate the location of the granules inside the representative volumes better, Figs. 1 and 2 show the section of the representative volume. The input data for all shown cases were set as follows. The target percentage of inclusion was 10 %, the minimal granule size was equal to 5 elements, and the maximal granule size was equal to 7 elements.

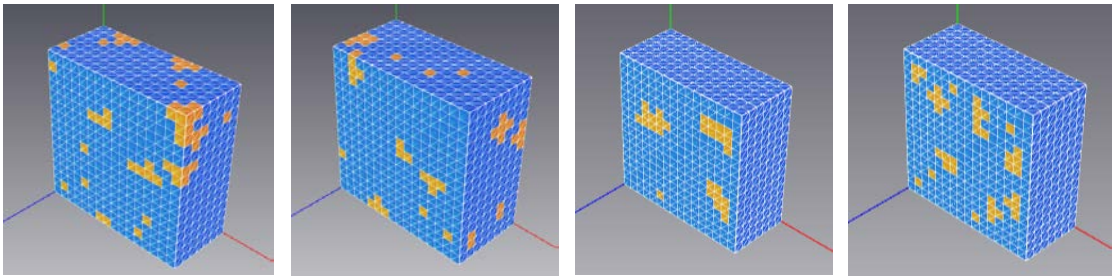

(*a*) (*b*) (*c*) (*d*)

Fig. 1. Examples of representative volumes for different versions of 3-0 algorithm: the domains with the size equal to 8

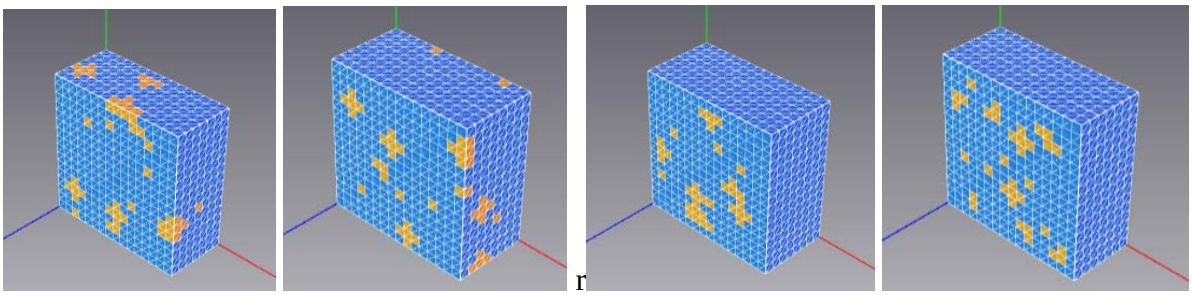

(*a*) (*b*) (*c*) (*d*)

Fig. 2. Examples of representative volumes for different versions of 3-0 algorithm: the domains with the size equal to 16

The key advantage to choose larger domain size is the absence of preset structure for the elements of the material 1 between separate domains. Figs. 1c and 1d demonstrate the regions of the main material without granules in the central part of the domain section. Besides, the generation accuracy increases with the decrease of the element size. During the domain generation, the overall proportion of inclusions changes discretely with the step equal to the ratio of the volume of a separate element to the total volume of the domain. For the generation of domain consisting of 512 elements, this step was equal to 1/512, or approximately 0.2 %, whereas in the case of the domain consisting of 4096 elements the step was equal to 0.025 %. In both cases, the algorithms without constrains (1a and 2a) ensure that the condition on the percentage of inclusions will be satisfied, but they do not ensure compliance with the condition on the granule size, as the granules can merge. In cases 1d and 2d, the condition for the granule size hold, but the target percentage of inclusions is not achieved. Table 1 summarizes the results of the granule generation for all described cases. For the case, when the inclusions are allowed to appear on the domain surface, 2b version of the algorithm is considered as optimal.

Table 1. Results of the representative volume generation using different cases and versions of the algorithm with the target percentage of inclusion equal to 10 % and the granule size in the range of 5 to 7 elements

Experiment case	Real percentage of inclusions, %	Real range of the granule size
1a	10	5-35
1b	10	5-19
1c	10	5-45
1d	9.3	5-7
2a	9.94	5-48
2b	10	5-7
2c	10	5-71
2d	9.91	5-7

We note that ACELAN-COMPOS package gives the user full statistics on the results for all cases of 3-0 algorithms, including the achieved percentage of inclusions, the range for the granule size, and the number of the generated granules of various sizes. Based on these results, the user can choose input data and the version of the algorithm, in order to obtain the best results for the representative volume generation.

5. Numerical examples

Let's consider the effect of various algorithms of granules formation in a representative volume on the effective material properties. PZT-4 piezoceramics with the following moduli

was used as the material of the first phase of composite $c_{11}^{E(1)} = 13.9 \cdot 10^{10}$; $c_{12}^{E(1)} = 7.78 \cdot 10^{10}$; $c_{13}^{E(1)} = 7.43 \cdot 10^{10}$; $c_{33}^{E(1)} = 11.5 \cdot 10^{10}$; $c_{44}^{E(1)} = 2.56 \cdot 10^{10}$ (N/m^2); $e_{31}^{(1)} = -5.2$; $e_{33}^{(1)} = 15.1$; $e_{15}^{(1)} = 12.7$ (C/m^2); $\varepsilon_{11}^{S(1)} = 730\varepsilon_0$; $\varepsilon_{33}^{S(1)} = 635\varepsilon_0$; $\varepsilon_0 = 8.85 \cdot 10^{-12}$ F/m (ε_0 is a dielectric constant of vacuum). Granules are more rigid inclusions from α-corundum (α–Al_2O_3). As in [16], we will consider α-corundum as an isotropic material with the following moduli: $c_{11}^{E(2)} = 46.88 \cdot 10^{10}$, $c_{12}^{E(2)} = 14.22 \cdot 10^{10}$ (N/m^2); $\varepsilon_{11}^{S(2)} = 10\varepsilon_0$.

Table 2 compares the material properties of composites with the same fraction of inclusions (10 %), but with different options for the formation of granules with a domain size of $8^3 = 512$ elements. The representative volume consisted of $16^3 = 4096$ elements granules that were formed in the range from 5 to 15 elements.

Table 2. Effective material properties of a piezocomposite with 10 % inclusions

	a) with no restrictions	b) without aggregation inside domains	c) without aggregation between domains	d) without any aggregation
% inclusions	10 %	10 %	10 %	10 %
$c_{11}^{E\text{eff}}, 10^{10}$, N/m^2	17.37	17.44	16.64	16.77
$c_{12}^{E\text{eff}}, 10^{10}$, N/m^2	8.61	8.65	8.45	8.47
$c_{13}^{E\text{eff}}, 10^{10}$, N/m^2	8.25	8.26	8.14	8.16
$c_{33}^{E\text{eff}}, 10^{10}$, N/m^2	15.41	15.67	15.10	14.98
$c_{44}^{E\text{eff}}, 10^{10}$, N/m^2	3.85	3.92	3.60	3.59
e_{31}^{eff}, C/m^2	-4.99	-4.96	-5.05	-5.04
e_{33}^{eff}, C/m^2	13.20	13.45	13.27	13.38
e_{15}^{eff}, C/m^2	11.62	11.60	11.58	11.68
$\varepsilon_{11}^{S\text{eff}} / \varepsilon_0$	638.58	643.16	634.88	639.97
$\varepsilon_{33}^{S\text{eff}} / \varepsilon_0$	548.39	559.23	552.29	555.13

Note that the relative differences between the values of the same type of moduli for various options of representative volumes, presented in Table 2, do not exceed 5 %. But such a small difference is observed only at small percentages of inclusions. Thus, Figure 3 shows a graph of changes in maximum relative discrepancies between the results of numerical experiments for effective elastic moduli $c_{11}^{E\text{eff}}$, $c_{12}^{E\text{eff}}$ and for permittivity coefficients $\varepsilon_{11}^{S\text{eff}}$, $\varepsilon_{33}^{S\text{eff}}$ for composites with fractions of inclusion from 5 to 30 %, and Fig. 4 presents similar graphs for piezoelectric moduli $e_{i\beta}^{\text{eff}}$ and $d_{i\beta}^{\text{eff}}$. Piezomoduli $d_{i\beta}^{\text{eff}}$ of considerable practical importance are determined through the found effective moduli by the formulas $d_{i\beta}^{\text{eff}} = e_{i\alpha}^{\text{eff}} s_{\alpha\beta}^{E\text{eff}}$, where $s_{\alpha\beta}^{E\text{eff}}$ are the coefficients of compliance matrix $\mathbf{s}^{E\text{eff}}$, which is inverse to the stiffness matrix $\mathbf{c}^{E\text{eff}}$: $\mathbf{s}^{E\text{eff}} = (\mathbf{c}^{E\text{eff}})^{-1}$. Since the piezoelectric moduli $d_{i\beta}^{\text{eff}}$ are computed using

additional operations with moduli $e_{i\beta}^{\text{eff}}$ and $c_{\alpha\beta}^{E\text{eff}}$, it can be expected that the maximum relative discrepancies for these moduli will be more significant.

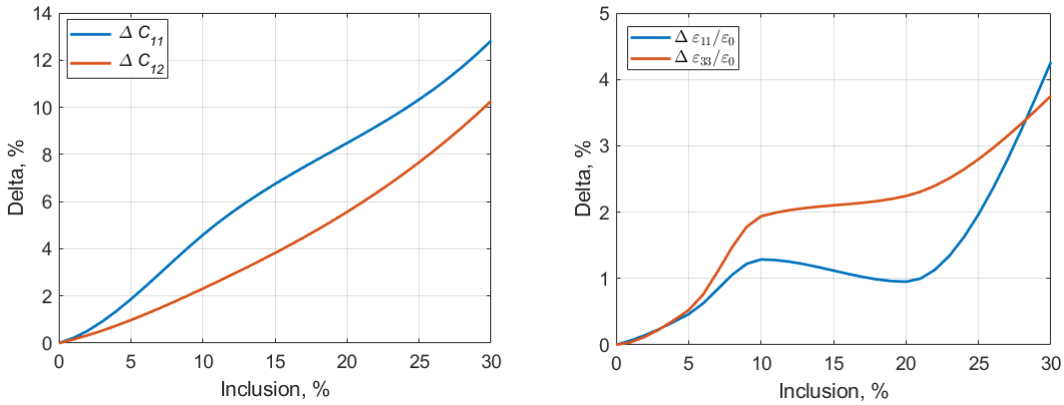

Fig. 3. Changes in the maximum relative difference in the values of the elastic stiffness moduli $c_{11}^{E\text{eff}}$, $c_{12}^{E\text{eff}}$ (left) and permittivities (right) obtained for various versions of 3-0 algorithms, depending on the fraction of inclusions

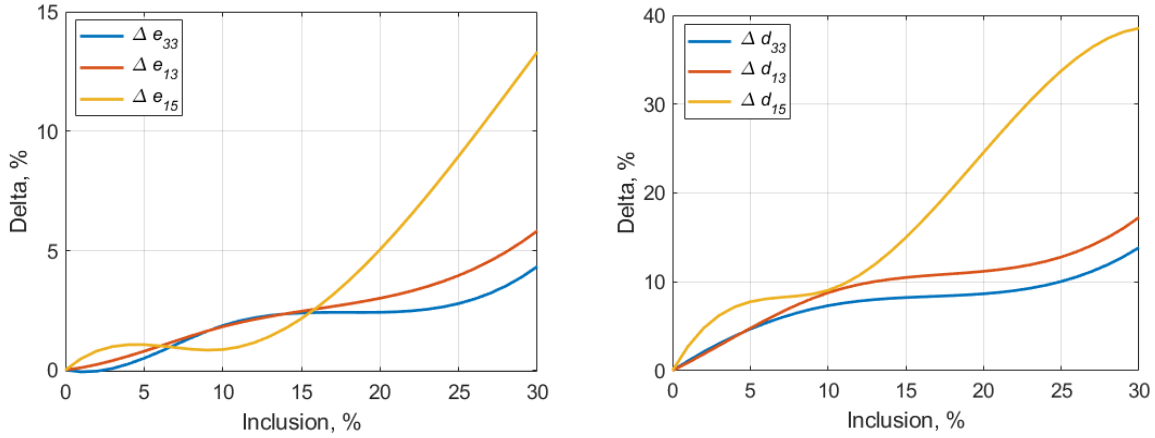

Fig. 4. Changes in the maximum relative difference in the values of the piezoelectric moduli $e_{i\beta}^{\text{eff}}$ (left) and $d_{i\beta}^{\text{eff}}$ (right) obtained for various variants of 3-0 algorithms, depending on the fraction of inclusions

As seen in Figures 3 and 4, for small percentages of inclusions (5-10 %), the effect of the granule formation algorithm on the final coefficient values is small. With an increase in the percentage of inclusions, the values of effective moduli differ more significantly. Moreover, nonmonotonicity, caused by various characteristics of the obtained granules, is observed in some subranges.

Thus, with large percentages of inclusions, there is a need to select an algorithm for generating representative volumes depending on the real structure of the composite. Inclusions can either have access to the surface of a representative volume, as in algorithms (*a*) and (*b*) or don't, as in algorithms (*c*) and (*d*). If inclusions are located inside the regular structure of the base material, the algorithms (*c*) and (*d*), with a domain size smaller than the size of a representative volume (series of experiments in Fig. 1), are better suited. If inclusions are combined into larger pores or granules during the manufacturing process of the

composite, algorithms (*a*) and (*c*) are preferred. The presented set of algorithms allows one to describe some variants of composites with inclusions or pores. However, for structures with a high percentage of inclusions, the choice of the algorithm may be limited by the maximum achievable percentage of inclusions. For example, the algorithm of version (*d*), due to strict restrictions on the isolation of inclusions and the connectivity of the base material, is not able to overcome the mark of 50 % of inclusions. This estimate can be increased by increasing the domain for generating a representative volume, which will increase the number of elements, the time of grid generation, and the total time of solving the identification problem. Currently, algorithms of versions (*a*) and (*b*) are used to generate materials with a high percentage of inclusions or highly porous materials. The difference in the coefficients obtained for representative volumes based on these algorithms does not exceed 6 % for elastic properties and 8 % for piezoelectric moduli.

Figures 5 and 6 provide graphs of effective material properties dependence in relation to the proportion of inclusions. The values of the characteristics, obtained for the most differing algorithms (*b*) and (*d*) with the same size of the representative volume ($16^3 = 4096$ elements) and the domain ($8^3 = 512$ elements), are estimated.

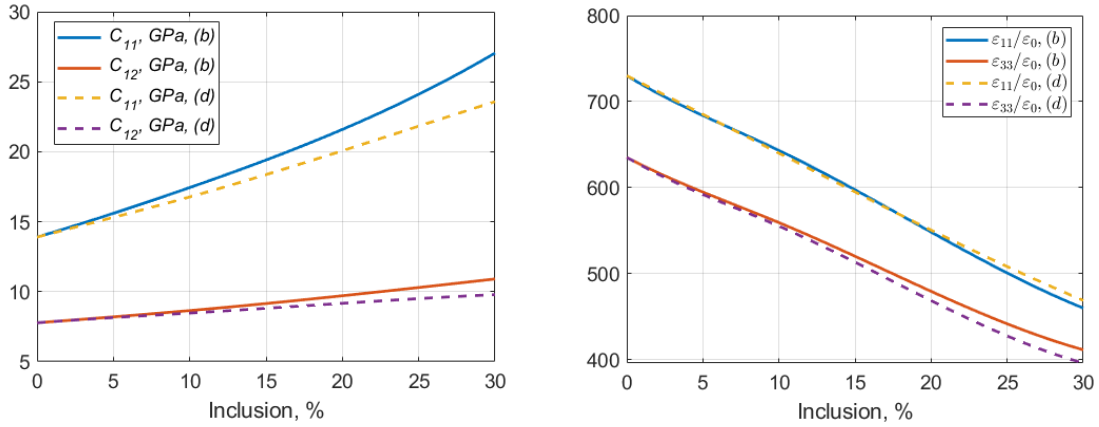

Fig. 5. Change in effective elastic properties (left) and dielectric constant (right) depending on the fraction of inclusions, for algorithms (*b*) and (*d*)

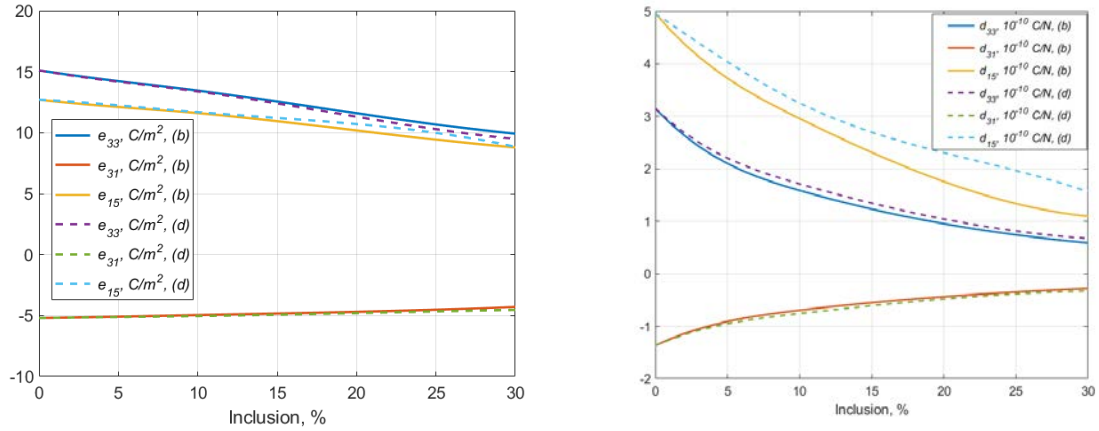

Fig. 6. Change of piezoelectric moduli $e_{i\beta}^{\text{eff}}$ (left) and $d_{i\beta}^{\text{eff}}$ (right) depending on the percentage of inclusions, for algorithms (*b*) and (*d*)

From Figures 5, 6 as well as from Figures 3, 4, it can be concluded, that the size of granules and their relative sizes significantly affect the effective moduli of piezocomposites at high percentages of inclusions. In this case, when varying granules generating algorithms, the stiffness moduli, permittivity coefficients, and piezoelectric moduli change in different ways.

6. Conclusions

So, the paper presents methods for determining the effective moduli of two-phase piezoelectric composites and an improved 3-0 algorithm for generating representative volume, implemented in the finite element package ACELAN-COMPOS. The algorithm allows adjusting the number of finite elements in a representative volume, the percentage and size of granules, both with the possibility of their adhesion to each other and with the prohibition of their adhesion.

Numerical experiments were carried out for piezoceramic composites with more rigid elastic inclusions. The results allow us to conclude that the improved 3-0 algorithm of the ACELAN-COMPOS package for generating representative volumes with isolated inclusions gives ample opportunity to vary not only the percentage of inclusions but also their relative sizes, which can be useful for precision computer-aided design of piezocomposites.

Acknowledgements. *The authors are grateful for the support of the Ministry of Science and Higher Education of the Russian Federation, project No. 9.1001.2017/4.6.*

References

[1] Ringgaard E, Lautzenhiser F, Bierregaard LM, Zawada T, Molz E. Development of porous piezoceramics for medical and sensor applications. *Materials*. 2015;8(12): 8877-8889.
[2] Rybyanets AN, Rybyanets AA. Ceramic piezocomposites: modeling, technology, and characterization. *IEEE Trans. Ultrason. Ferroelectr. Freq. Control*. 2011;58(9): 1757-1773.
[3] Rybianets AN, Nasedkin AV, Turik AV. New microstructural design concept for polycrystalline composite material. *Integrated Ferroelectrics*. 2004;63(1): 179-182.
[4] Banno H. Effect of shape and volume fraction of closed pores on dielectric, elastic and electromechanical properties of dielectric and piezoelectric ceramics - a theoretical approach. *Amer. Ceram. Soc. Bull*. 1987;66(9): 1332-1337.
[5] Iyer S, Venkatesh TA. Electromechanical response of porous piezoelectric materials: Effects of porosity connectivity. *Appl. Phys. Lett*. 2010;97(7): 072904.
[6] Iyer S, Venkatesh TA. Electromechanical response of (3–0) porous piezoelectric materials: Effects of porosity shape. *J. Appl. Phys*. 2011;110(3): 034109.
[7] Iyer S, Venkatesh TA. Electromechanical response of (3–0, 3–1) particulate, fibrous, and porous piezoelectric composites with anisotropic constituents: A model based on the homogenization method. Int. J. Solids Struct. 2014;51(6): 1221-1234.
[8] Kar-Gupta R, Venkatesh TA. Electromechanical response of porous piezoelectric materials: Effects of porosity distribution. *Appl. Phys. Lett*. 2007;91(6): 062904.
[9] Nguyen BV, Challagulla KS, Venkatesh TA, Hadjiloizi DA, Georgiades AV. Effects of porosity distribution and porosity volume fraction on the electromechanical properties of 3-3 piezoelectric foams. *Smart Mater. Struct*. 2016;25(12): 125028.
[10] Pan'kov AA. Correlation functions and piezoelectromagnetic properties of structures determined by the method of correlation components. *Mech. Compos. Mater*. 2015;50(6): 681-694.
[11] Semenov AS. Micromechanical model of a polycrystalline ferroelectrelastic material with consideration of defects. *J. Appl. Mech. Tech. Phys*. 2019;60(6): 1125-1140.
[12] Gerasimenko TE, Kurbatova NV, Nadolin DK, Nasedkin AV, Nasedkina AA, Oganesyan PA, Skaliukh AS, Soloviev AN. Homogenization of piezoelectric composites with

internal structure and inhomogeneous polarization in ACELAN-COMPOS finite element package. In: Sumbatyan MA. (ed.) *Wave Dynamics, Mechanics and Physics of Microstructured Metamaterials. Advanced Structured Materials*. Advanced Structured Materials book series (STRUCTMAT, volume 109). Singapore: Springer; 2019. p.113-131.
[13] Kurbatova NV, Nadolin DK, Nasedkin AV, Oganesyan PA, Soloviev AN. Finite element approach for composite magneto-piezoelectric materials modeling in ACELAN-COMPOS package. In: Altenbach H, Carrera E, Kulikov G. (eds.) *Analysis and Modelling of Advanced Structures and Smart Systems*. Advanced Structured Materials book series (STRUCTMAT, volume 81). Singapore: Springer; 2018. p.69-88.
[14] Kurbatova NV, Nadolin DK, Nasedkin AV, Nasedkina AA, Oganesyan PA, Skaliukh AS, Soloviev AN. Models of active bulk composites and new opportunities of ACELAN finite element package. In: Sumbatyan MA. (ed.) *Wave Dynamics and Composite Mechanics for Microstructured Materials and Metamaterials*. Advanced Structured Materials book series (STRUCTMAT, volume 59). Singapore: Springer; 2017. p.133-158.
[15] Newnham RE, Skinner DP, Cross LE. Connectivity and piezoelectric-pyroelectric composites. *Mater. Res. Bull*. 1978;13: 525-536.
[16] Kudimova AB, Mikhayluts IV, Nadolin DK, Nasedkin AV, Nasedkina AA, Oganesyan PA, Soloviev AN. Computer design of porous and ceramic piezocomposites in the finite element package ACELAN. *Procedia Structural Integrity*. 2017;6: 301-308.
[17] Kudimova AB, Nadolin DK, Nasedkin AV, Nasedkina AA, Oganesyan PA, Soloviev AN. Models of porous piezocomposites with 3-3 connectivity type in ACELAN finite element package. *Mater. Phys. Mech*. 2018;37(1): 16-24.
[18] Kudimova AB, Nadolin DK, Nasedkin AV, Oganesyan PA, Soloviev AN. Finite element homogenization models of bulk mixed piezocomposites with granular elastic inclusions in ACELAN package. *Mater. Phys. Mech*. 2018;37(1): 25-33.
[19] Nasedkin AV, Shevtsova MS. Improved finite element approaches for modeling of porous piezocomposite materials with different connectivity. In: Parinov IA. (ed.) *Ferroelectrics and superconductors: Properties and applications*. New York: Nova Science Publishers; 2011. p.231-254.
[20] Benzi M, Golub GH, Liesen J. Numerical solution of saddle point problems. *Acta Numerica*. 2005;14: 1-137.
[21] Vanderbei RJ. Symmetric quasidefinite matrices. *SIAM J. Optim*. 1995;5(1):100-113.
[22] Paige CC, Saunders MA. Solution of sparse indefinite systems of linear equations. *SIAM J. Numer. Anal*. 1975;12(4): 617-629.
[23] Paige CC, Saunders MA. LSQR: An algorithm for sparse linear equations and sparse least squares. *ACM Trans. Math. Software*. 1982;8(1): 43-71.
[24] Davis TA. *Direct methods for sparse linear systems*. Philadelphia, PA: SIAM; 2006.
[25] Hellen TK. Effective quadrature rules for quadratic solid isoparametric finite elements. *Int. J. Num. Meth. Eng*. 1972;4(4): 597-600.